Biochemical and Biophysical Research Communications 456 (2015) 733–736

Contents lists available at ScienceDirect

Biochemical and Biophysical Research Communications

journal homepage: www.elsevier.com/locate/ybbrc

Binding mode of the oxidized α-anomer of NAD$^+$ to RSP, a Rex-family repressor

Yingying Zheng [a,1], Tzu-Ping Ko [b,1], Yunyun Yang [c,a], Weilan Shao [d,*], Rey-Ting Guo [a,*]

[a] Industrial Enzymes National Engineering Laboratory, Tianjin Institute of Industrial Biotechnology, Chinese Academy of Sciences, Tianjin 300308, China
[b] Institute of Biological Chemistry, Academia Sinica, Taipei 11529, Taiwan
[c] College of Biotechnology, Tianjin University of Science and Technology, Tianjin 300457, China
[d] Biofuels Institute, School of Environment, Jiangsu University, Zhenjiang 212013, China

ARTICLE INFO

Article history:
Received 28 November 2014
Available online 16 December 2014

Keywords:
Transcription regulation
Ethanol fermentation
Thermoanaerobacter ethanolicus
Allosteric effector

ABSTRACT

The Rex-family repressors sense redox levels by alternative binding to NADH or NAD$^+$. RSP is the homologue of Rex in *Thermoanaerobacter ethanolicus* JW200^T and regulates ethanol fermentation in this obligate anaerobe. The dimeric repressor binds to DNA by an open conformation. The crystal structure of RSP/α-NAD$^+$ complex shows a different set of ligand interactions mainly due to the unique configuration of the nicotinamide moiety. The positively charged ring is covered by the Tyr102 side chain and interacts with a sulfate ion adjacent to the N-terminus of helix α8. Consequently, the RSP dimer may be locked in a closed conformation that does not bind to DNA. However, α-NAD$^+$ does not show a higher affinity to RSP than β-NAD$^+$. It has to be improved for possible use as an effector in modulating the repressor.

1. Introduction

The Rex-family repressors are negative regulatory proteins that control the expression of genes in respiratory metabolic pathways [1]. By alternatively binding to either NAD$^+$ or NADH in the C-terminal Rossmann-fold domain, the homodimeric Rex assumes a flexible open conformation that allows DNA binding to the N-terminal winged-helix domain, or a more rigid closed conformation that does not bind to DNA [2–5]. In this way, Rex directly senses the NADH and NAD$^+$ concentrations as a redox state indicator, and actively modulates the metabolic pathways at the transcription level. In *Thermoanaerobacter ethanolicus* the Rex ortholog is termed RSP (for redox sensing protein). It binds to palindromic sequences in the transcription regulation regions (TRR) of ethanol fermentation gene operons *adhA*, *adhB* and *adhE* (Fig. 1) [6].

The mechanism of anaerobic RSP regulation is similar to the aerobic Rex system while showing a number of variations. Previously we showed that in the RSP/DNA/β-NAD$^+$ complex, each monomer in the RSP dimer contains a bound β-NAD$^+$ [7]. When there is plenty of NADH, it replaces NAD$^+$ in the same binding site (Fig. 1). The nicotinamide shows a *syn* orientation in β-NAD$^+$, which is different from the *anti* orientation in β-NADH. The interactions between RSP and β-NADH trigger movements of the swapped C-terminal helices α8a/α8b and make the repressor into a closed conformation. Interestingly, NADH binds to RSP as a β-anomer despite the use of α-NADH in co-crystallization, presumably due to rapid epimerization (Zheng et al., unpublished data). In contrast, the oxidized α-NAD$^+$ does not epimerize into β-NAD$^+$ [8]. Enzymatic oxidation of α-NADH has been reported [9], whereas the accumulation of α-NAD$^+$ would lead to continual loss of cellular redox currency [10].

To investigate the possible role of α-NAD$^+$ in redox regulation, we co-crystallized RSP with α-NAD$^+$ and determined the complex structure by X-ray diffraction. The RSP dimer turned out to be in the closed conformation, with the nicotinamide moiety of α-NAD$^+$ disposed in a different way from those of β-NAD$^+$ and β-NADH. We also compared the affinity of RSP to both anomers of NAD$^+$ by using isothermal titration calorimetry (ITC).

2. Materials and methods

2.1. Determination of the RSP/α-NAD$^+$ structure

The RSP protein was expressed by using the plasmid pET28a-RSP in *Escherichia coli* BL21 (DE3) and purified as described previously

* Corresponding authors at: Biofuels Institute, School of Environment, Jiangsu University, 301 Xuefu Road, Zhenjiang 212013, China. Fax: +86 025 85891836 (W. Shao). Tianjin Institute of Industrial Biotechnology, Chinese Academy of Sciences, Room A507, 32 Xi Qi Dao, Tianjin Airport Economic Zone, Tianjin 300308, China. Fax: +86 022 24828701 (R.-T. Guo).

E-mail addresses: weilanshao@gmail.com (W. Shao), guo_rt@tib.cas.cn (R.-T. Guo).

[1] YZ and TPK contributed equally to this work.

http://dx.doi.org/10.1016/j.bbrc.2014.12.049
0006-291X/

[7]. The expression was induced by adding IPTG and continued for 6 h at 30 °C. The protein was purified by a heat treatment and a chromatography on DEAE Sepharose, and concentrated to 10 mg ml^{-1} after $(NH_4)_2SO_4$ precipitation and dialysis against 150 mM NaCl, 25 mM Tris pH 7.5. The RSP/α-NAD$^+$ crystals were obtained by sitting drop method at 25 °C with 5 mM α-NAD$^+$ added to the protein solution and a reservoir solution of 20% w/v polyethylene glycol (PEG) 3350, 0.4 M $(NH_4)_2SO_4$ and 0.1 M Bis–Tris pH 5.5. X-ray diffraction data were collected at the National Synchrotron Radiation Research Center (NSRRC; BL13B1) in Hsinchu, Taiwan, and processed by using HKL2000 [11]. The crystal did not need a cryoprotectant.

Using the *apo*-form RSP (PDB: 3WG9) as a search model, the crystal structure was determined by molecular replacement (MR). The space group is $P2_12_12$ with one RSP dimer in an asymmetric unit. The program CNS [12] was used for MR calculations as well as subsequent computational refinement. Manual adjustment of the model was carried out by using Coot [13,14]. The structure was further refined by using REFMAC5 with TLS and isotropic temperature factors [15]. Structural analysis, comparison and presentation employed the programs Coot [13], MolProbity [16] and PyMOL (http://pymol.sourceforge.net/). Some data collection and refinement statistics can be found in Table 1.

Table 1
Statistics of the RSP/α-NAD$^+$ crystal.

Data collection	
Space group	$P2_12_12$
Unit cell *a*, *b*, *c* (Å)	139.8, 74.1, 54.8
Resolution (Å)[a]	25–2.10 (2.18–2.10)
Unique reflections	33,930 (3243)
Average redundancy	5.0 (4.7)
Completeness (%)	99.4 (96.6)
Average $\langle I\rangle/\langle\sigma(I)\rangle$	20.7 (2.5)
R_{merge} (%)	7.2 (45.6)
Wilson *B* factor (Å^2)	31.3
Refinement	
No. of reflections[b]	32,146 (2834)
R_{work} (95% data)	0.179 (0.218)
R_{free} (5% data)	0.231 (0.284)
RMSD bonds (Å)	0.0169
RMSD angles (°)	1.82
Ramachandran (%)	
Favored/allowed/outliers	96.0/3.1/0.9
$B_{average}$ (Å^2)/atoms	
Protein	35.4/3430
Cofactor	33.1/88
Water	51.4/418
Ions	60.6/30
PDB code	3WGG

[a] Numbers in parentheses are for the outermost resolution shells.
[b] All positive reflections were used in the refinement.

2.2. Affinity measurement with ITC

All samples of the ITC experiments were prepared in a buffer of 50 mM 2-(N-morpholino)ethanesulfonic acid (MES) pH 6.5 and freshly degassed right before use. All titrations were performed at 25 °C and a stirring speed of 60 rpm, using TAM III isothermal calorimeter (TA Instruments-Waters LLC, USA). The reaction cell was filled with 850 μl RSP solution at a concentration of 80 μM. The titrated α/β-NAD$^+$ concentration was 1 mM. Raw data were processed and fitted by using the software NanoAnalyze supplied with the instrument, and a best fit of the data was obtained by using a single set of independent binding model. The background was subtracted using the average data points of the last few sample injections, which approximated saturation. The dilution heat of titrant was also assessed by injecting the ligands into the buffer. In both cases it was relatively small and constant.

3. Results

3.1. The closed RSP/α-NAD$^+$ structure

Although by employing a similar reservoir solution, the RSP/α-NAD$^+$ complex crystallized in a different space group from that of the *apo*-form crystal. The former contains one RSP dimer in an asymmetric unit, whereas the latter contains two. All three dimers show a closed conformation, with RMSD of about 0.7 Å between the Cα-atoms (Fig. S1). Each RSP monomer contains a bound dinucleotide on the C-terminal end of the parallel β-sheet in the Rossmann fold domain (Fig. S2). The adenine ring binds to a nonpolar pocket lined by Ile90, Ile118, Val135, Ile154 and Pro155 near the protein surface (Fig. 2A). It is sandwiched between the side chains

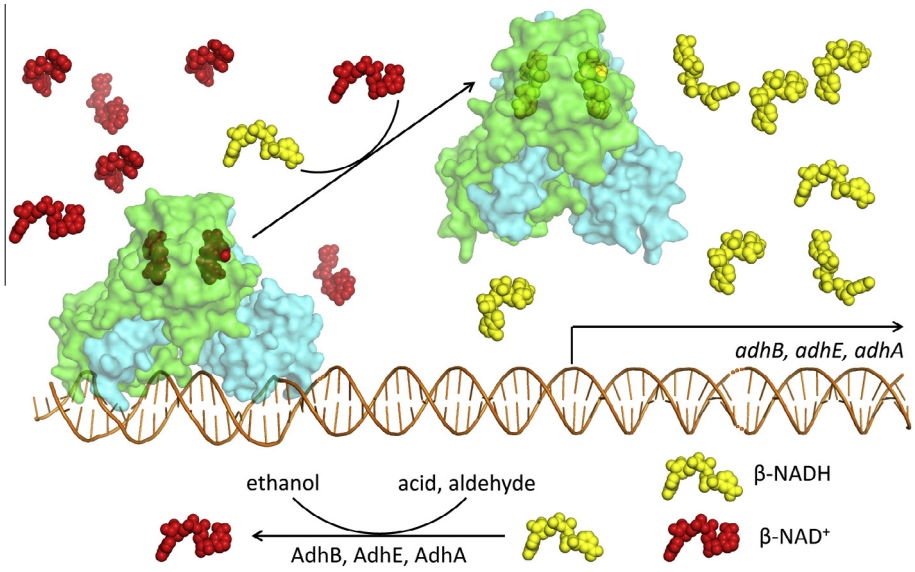

Fig. 1. Metabolic regulation by RSP. The genes *adhA*, *adhB* and *adhE* involved in ethanol production are repressed by RSP binding to their operator regions. When plenty of NADH is present, it binds to RSP and results in gene induction.

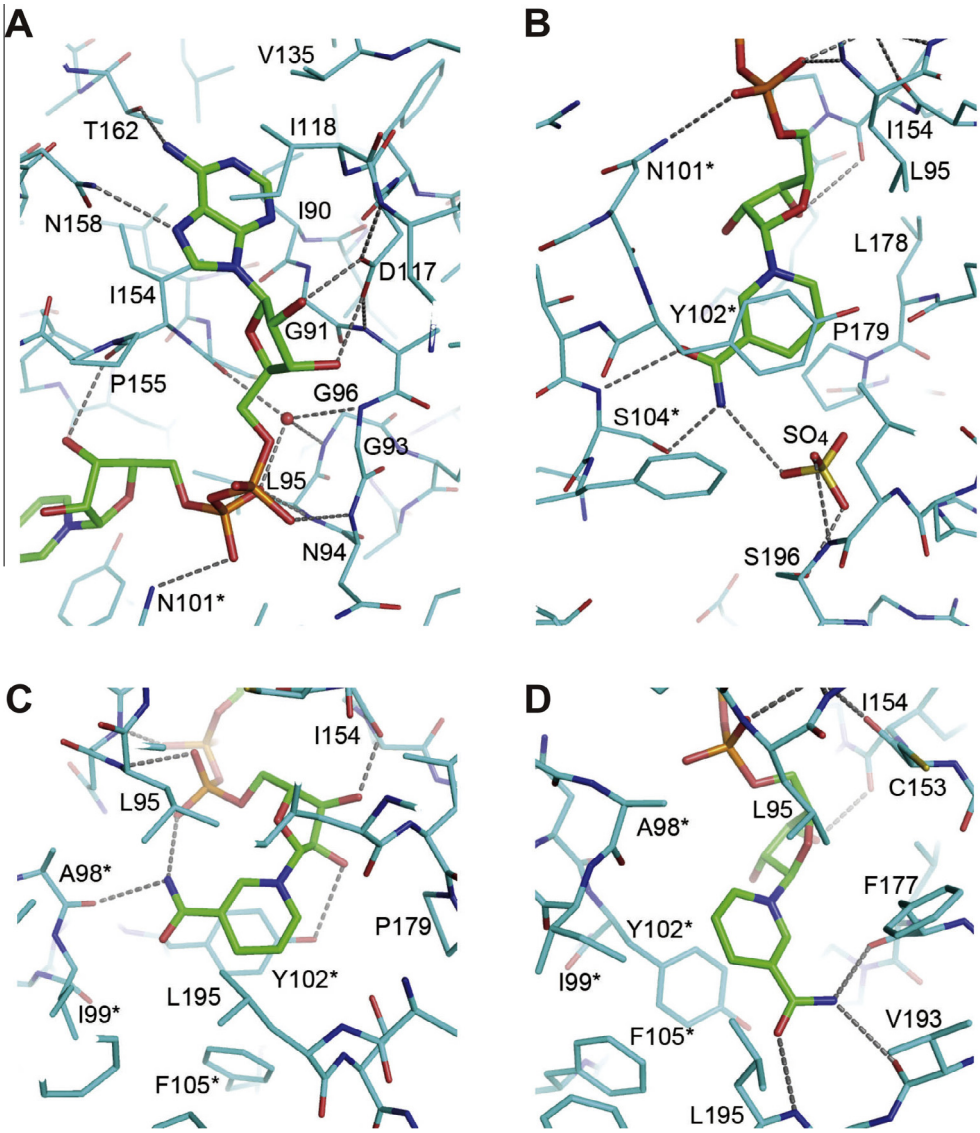

Fig. 2. RSP interactions with NAD. The dinucleotide is shown as a thick stick model with green carbon atoms, and the protein as a thin stick model with cyan carbons. Hydrogen bonds are indicated by gray dashed lines. In (A) the view is centered on the adenosine and pyrophosphate moieties in the RSP/α-NAD^+ complex. The red sphere indicates a mediating water molecule. In (B) the view is switched to the nicotinamide and ribose parts. Here a sulfate ion is also shown. The corresponding parts in the RSP/DNA/β-NAD^+ (PDB: 3WGI) and RSP/β-NADH (PDB: 3WGH) complexes are shown in (C) and (D). All amino acid residues involved in the interactions are labeled. (For interpretation of the references to color in this figure legend, the reader is referred to the web version of this article.)

of Ile118 and Ile154, and presumably stabilized by strong van der Waals (VDW) interactions. Besides, the N6 and N7 form hydrogen bonds with Thr162 (OG1) and Asn158 (ND2). The A-ribose ring shows VDW interactions with Gly91 and Pro155, and its 2′-OH and 3′-OH form hydrogen bonds with the side chain of Asp117, which is further bound to Ala92 and Asn119.

The pyrophosphate of α-NAD^+ binds to the N-terminal end of helix α5a, forming two hydrogen bonds with the backbone N of Asn94 and Leu95. It is also bound to the side chain ND2 of Asn101* from the other monomer (designated by an asterisk) and a buried water molecule with low temperature factor, which is held by Gly93, Gly96 and Cys153. The 3′-OH of N-ribose is hydrogen bonded to the backbone O of Ile154 and the sugar ring is in VDW contacts with the Leu95 and Leu178 side chains (Fig. 2B). The nicotinamide ring, which shows an *anti* orientation, stacks with the Tyr102* side chain. On the other side it is in contact with Pro179. Its amide group forms two hydrogen bonds to Ser104* (N and OG). Interestingly, the amide N7 is bound to a sulfate ion, which also interacts with the positively charged ring at a distance of 3.4 Å and makes two HBs to Ser196 (N and OG) at the N-terminus of helix α8a.

3.2. NAD^+ affinity to RSP

The absorption spectrum of RSP did not show a peak for NAD at 340 nm, and the peak at 280 nm did not shift to lower wavelengths, indicating that the protein did not co-purify with bound dinucleotide. Previous attempts to co-crystallize RSP with β-NAD^+ were not successful, while complex crystals with α-NAD^+ were obtained first. Therefore it is intriguing to find out if α-NAD^+ actually binds to RSP in solution. By using ITC, the dissociation equilibrium constant (K_D) of α-NAD^+ and RSP was measured as 39.9 μM. For comparison, the K_D of β-NAD^+ and RSP was also measured and found to be 17.6 μM (Fig. S3). The large negative enthalpy change (ΔH) in comparison with the entropy change (ΔS; Table 2) indicates that both α-NAD^+ and β-NAD^+ binding are

Table 2
Thermodynamic components from ITC measurements.

	K_A (M^{-1})	K_D (μM)	ΔG (kJ/mol)	ΔH (kJ/mol)	$-T\Delta S$ (kJ/mol)
α-NAD$^+$	25,084	39.9	−25.1	−23.7	−1.4
β-NAD$^+$	56,936	17.6	−27.1	−32.8	5.7

mostly enthalpy-driven. However, a small positive entropic contribution is also observed for α-NAD$^+$.

4. Discussion

T. ethanolicus JW200 is an obligate anaerobe that ferments glucose and xylose into ethanol and CO_2. Unlike those in aerobic organisms, the RSP-regulated genes are not involved in oxidative phosphorylation but related to alcohol dehydrogenases [6]. In general, a Rex-family protein is flexible as a free dimer, or when bound to β-NAD$^+$. It binds to operator DNA at low NADH levels. At higher NADH levels, due to the 20,000 times stronger affinity of NADH than NAD$^+$, NADH replaces NAD$^+$ in the binding pocket [4]. It was shown that the *in vitro* transcription of *adhB* was repressed by RSP but recovered by adding NADH [6]. In the RSP/DNA/β-NAD$^+$ complex, the *syn*-nicotinamide of β-NAD$^+$ interacts with the pyrophosphate group and amino acids from both monomers, including Tyr102* (Fig. 2C). In the RSP/NADH complex, the uncharged *anti*-nicotinamide of β-NADH is surrounded by more non-polar amino acid residues at the dimer interface and also stacked with Tyr102* (Fig. 2D). Interestingly, the relative dispositions of Tyr102* are both different from that in the RSP/α-NAD$^+$ complex (Fig. 2B).

The difference can be attributed largely to the binding modes of the N-ribose and nicotinamide moieties, especially the latter. The nicotinamide of α-NAD$^+$ is bound in an extended conformation (*anti*) and sandwiched between Pro179 and Tyr102*, which also shields the nicotinamide from the bulk solvent (Fig. 2B). In β-NAD$^+$, the nicotinamide turns back (*syn*) to form a hydrogen bond with the pyrophosphate and stacks only on one side with Tyr102*, while the other side is partially exposed to solvent (Fig. 2C). The uncharged, high-affinity β-NADH binds to RSP with more nonpolar interactions, but the nicotinamide is not covered by Tyr102* (Fig. 2D). The interactions may account for an unfavorable entropy component (ΔS) of β-NAD$^+$ binding in comparison with α-NAD$^+$. As a natural "substrate", β-NAD$^+$ may bind to RSP by rapid equilibrium between bound and unbound forms, suggesting an "induced-fit" mode of binding, whereas α-NAD$^+$ as an "analogue" appears to bind in a more rigid, "lock-and-key" manner.

As shown above, the binding mode of α-NAD$^+$ in the crystal also used a sulfate ion to bridge the positively charged nicotinamide ring and the N-terminal dipole of helix α8a, resulting in a similar closed conformation to that of RSP/NADH complex. However, α-NAD$^+$ made fewer direct bonds to the protein than did β-NAD$^+$, and the absence of sulfate in the solution of ITC experiments further reduced the number of indirect bonds to α-NAD$^+$, resulting in a smaller ΔH. The presence of MES in the buffer of ITC may have some effects against α-NAD$^+$ binding. Not only does the sulfonate part resemble the bound sulfate but the morpholine moiety can also mimic the nicotinamide ring, making MES a competitive antagonist of α-NAD$^+$ (Fig. S4).

Previous soaking experiments of *apo*-RSP crystals with β-NAD$^+$ yielded poor X-ray diffraction data sets with electron densities for the ADP moiety only, and so did cocrystallization (results not shown). In both cases the RSP dimer adopted the closed conformation. On the other hand, Rex from *Bacillus subtilis* with bound NADH or ATP showed an extended conformation in which the N terminal domain was stretched out and the nicotinamide-ribose moiety was not seen [4]. Due to the similar affinity of α-NAD$^+$ and β-NAD$^+$, it is not likely for α-NAD$^+$ alone to displace β-NAD$^+$ or NADH. However, by taking the mediating sulfate ion into account, it may be possible to design an artificial nicotinamide–ribonucleoside and sulfonate-based inducer which would not interfere with other NAD-dependent metabolic processes. It probably does not need the ADP moiety which is readily available *in vivo*. The inducer can be used in a similar way to using IPTG in controlling the lac operon, for example, but producing more ethanol in the fermentation process by *T. ethanolicus*.

Acknowledgments

We thank Dr. Jie Shen for advice on ITC experiments, and the National Synchrotron Radiation Research Center of Taiwan for beam time allocation and data collection assistance. This work was supported by grants from the National High Technology Research and Development Program of China (2012AA022200), the National Natural Science Foundation of China (31170027, 31200053, 31300615 and 31400678) and Key Research Program of the Chinese Academy of Sciences Grant (KSZD-EW-Z-015-2).

Appendix A. Supplementary data

Supplementary data associated with this article can be found, in the online version, at http://dx.doi.org/10.1016/j.bbrc.2014.12.049.

References

[1] D. Brekasis, M.S. Paget, A novel sensor of NADH/NAD$^+$ redox poise in *Streptomyces coelicolor* A3(2), EMBO J. 22 (2003) 4856–4865.
[2] E.A. Sickmier, D. Brekasis, S. Paranawithana, J.B. Bonanno, M.S. Paget, S.K. Burley, C.L. Kielkopf, X-ray structure of a Rex-family repressor/NADH complex insights into the mechanism of redox sensing, Structure 13 (2005) 43–54.
[3] A. Nakamura, A. Sosa, H. Komori, A. Kita, K. Miki, Crystal structure of TTHA1657 (AT-rich DNA-binding protein; p25) from *Thermus thermophilus* HB8 at 2.16 Å resolution, Proteins 66 (2007) 755–759.
[4] E. Wang, M.C. Bauer, A. Rogstam, S. Linse, D.T. Logan, C. von Wachenfeldt, Structure and functional properties of the *Bacillus subtilis* transcriptional repressor Rex, Mol. Microbiol. 69 (2008) 466–478.
[5] K.J. McLaughlin, C.M. Strain-Damerell, K. Xie, D. Brekasis, A.S. Soares, M.S. Paget, C.L. Kielkopf, Structural basis for NADH/NAD$^+$ redox sensing by a Rex family repressor, Mol. Cell 38 (2010) 563–575.
[6] J. Pei, Q. Zhou, Q. Jing, L. Li, C. Dai, H. Li, J. Wiegel, W. Shao, The mechanism for regulating ethanol fermentation by redox levels in *Thermoanaerobacter ethanolicus*, Metab. Eng. 13 (2011) 186–193.
[7] Y. Zheng, T.P. Ko, H. Sun, C.H. Huang, J. Pei, R. Qiu, A.H. Wang, J. Wiegel, W. Shao, R.T. Guo, Distinct structural features of Rex-family repressors to sense redox levels in anaerobes and aerobes, J. Struct. Biol. 188 (2014) 195–204.
[8] N.J. Oppenheimer, N.O. Kaplan, The alpha beta epimerization of reduced nicotinamide adenine dinucleotide, Arch. Biochem. Biophys. 166 (1975) 526–535.
[9] N.J. Oppenheimer, The stereospecificity of oxidation of α-[4R-2H]NADH by dehydrogenases, J. Biol. Chem. 261 (1986) 12209–12212.
[10] B.A. Beaupre, M.R. Hoag, B.R. Carmichael, G.R. Moran, Kinetics and equilibria of the reductive and oxidative half-reactions of human renalase with α-NADPH, Biochemistry 52 (2013) 8929–8937.
[11] Z. Otwinowski, W. Minor, Processing of X-ray diffraction data collected in oscillation mode, Methods Enzymol. 276 (1997) 307–326.
[12] A.T. Brünger, P.D. Adams, G.M. Clore, W.L. DeLano, P. Gros, R.W. Grosse-Kunstleve, J.S. Jiang, J. Kuszewski, M. Nilges, N.S. Pannu, R.J. Read, L.M. Rice, T. Simonson, G.L. Warren, Crystallography & NMR system: a new software suite for macromolecular structure determination, Acta Crystallogr. D Biol. Crystallogr. 54 (1998) 905–921.
[13] P. Emsley, B. Lohkamp, W.G. Scott, K. Cowtan, Features and development of Coot, Acta Crystallogr. D Biol. Crystallogr. 66 (2010) 486–501.
[14] Collaborative Computational Project, Number 4, The CCP4 suite: programs for protein crystallography, Acta Crystallogr. D Biol. Crystallogr. 50 (1994) 760–763.
[15] G.N. Murshudov, P. Skubák, A.A. Lebedev, N.S. Pannu, R.A. Steiner, R.A. Nicholls, M.D. Winn, F. Long, A.A. Vagin, REFMAC5 for the refinement of macromolecular crystal structures, Acta Crystallogr. D Biol. Crystallogr. 67 (2011) 355–367.
[16] V.B. Chen, W.B. Arendall 3rd, J.J. Headd, D.A. Keedy, R.M. Immormino, G.J. Kapral, L.W. Murray, J.S. Richardson, D.C. Richardson, MolProbity: all-atom structure validation for macromolecular crystallography, Acta Crystallogr. D Biol. Crystallogr. 66 (2010) 12–21.